International Journal of Bifurcation and Chaos, Vol. 26, No. 5 (2016) 1650082 (12 pages)

DOI: 10.1142/S0218127416500826

An. Figs. 1, 3, 7, 8
- higher resolution
images available

# Bifurcation Analysis of a Power System Model with Three Machines and Four Buses

Yu Chang* and Xiaoli Wang†
*Department of Mathematics,*
*Beijing University of Chemical Technology,*
*Beijing 100029, P. R. China*
**changyu@mail.buct.edu.cn*
†*759212592@qq.com*

Dashun Xu
*Department of Mathematics,*
*Southern Illinois University,*
*Carbondale, IL 62901, USA*
*dashunxu@siu.edu*

Received ; Revised

The bifurcation phenomena in a power system with three machines and four buses are investigated by applying bifurcation theory and harmonic balance method. The existence of saddle-node bifurcation and Hopf bifurcation is analyzed in time domain and in frequency domain, respectively. The approach of the fourth-order harmonic balance is then applied to derive the approximate expressions of periodic solutions bifurcated from Hopf bifurcations and predict their frequencies and amplitudes. Since the approach is valid only in some neighborhood of a bifurcation point, numerical simulations and the software Auto2007 are utilized to verify the predictions and further study bifurcations of these periodic solutions. It is shown that the power system may have various types of bifurcations, including period-doubling bifurcation, torus bifurcation, cyclic fold bifurcation, and complex dynamical behaviors, including quasi-periodic oscillations and chaotic behavior. These findings help to better understand the dynamics of the power system and may provide insight into the instability of power systems.

*Keywords*: Bifurcation; frequency domain; harmonic balance; power system.

## 1. Introduction

One major concern of power systems is about their instability. The analysis of power system models demonstrates that instability of power systems may be triggered by static bifurcation (saddle-node bifurcation) and dynamic bifurcations (Hopf bifurcation, torus bifurcation, cyclic fold bifurcation, period-doubling bifurcation). Therefore, the bifurcation analysis of power systems has attracted many researchers' attention [Abed *et al.*, 1993; Kwatny *et al.*, 1995; Jing *et al.*, 2002; Ayasun *et al.*, 2004; Wang *et al.*, 2014; Pirooz *et al.*, 2015] and has been studied through different approaches. Harb and Jabbar [2003] applied the global state feedback linearization (GLC) to a small power system and proposed a strategy to control the Hopf bifurcation and chaos. Applying bifurcation theory, Li *et al.* [2008] provided optimal placements of measurement

*Author for correspondence; Address for correspondence: Department of Mathematics, Beijing University of Chemical Technology, 15 beisanhuan east road, chaoyang district, Beijing 100029, P. R. China.

devices for a power system load model. Rakshit *et al.* [2010] developed a systematic approach to analyze border collision bifurcations in a static VAR compensator. Zhang and Chiang [2011] numerically studied the local bifurcation bounding and steady-state security boundary in large electric power systems. Sangrody *et al.* [2012] utilized modified Poincaré map, Lyapunov exponents and bifurcation diagram to investigate the bifurcation and chaos in scalar drives of induction machines. Huang *et al.* [2013] reported a low-frequency oscillation emerging from Hopf bifurcation in three-phase PFC (power-factor-correction) power supplies, and further developed a model of the grid-converter system to illustrate the low-frequency instability. Through multiparameter bifurcation analysis, the effect of degenerate Hopf bifurcations on the voltage stability was numerically studied by Mendoza-Armenta *et al.* [2013].

This work considers a power system with three machines and four buses. The system can be modeled by swing equations [Kwatny & Yu, 1989]. The structure of equilibria of the system without damping has been studied by Tavora and Smith [1972] and Kwatny *et al.* [1995] through different methods. In the case of no damping, Kwatny and Yu [1989] studied the properties of energy functions near Hopf bifurcation points and explained flutter instability (one of typical instabilities in power systems). For the system with damping, Kwatny and Piper [1990] utilized the approach of frequency domain analysis to analyze Hopf bifurcation. Chang [2002] provided the sufficient conditions for the existence of the saddle-node bifurcation and Hopf bifurcation in time domain, and numerically analyzed the bifurcations and dynamical behaviors of the power system.

As mentioned by Kwatny and Piper [1990], flutter instability of a power system is typically accompanied by the occurrence of Hopf bifurcation, and hence periodic oscillations resulting from Hopf bifurcation deserve one's careful attention. Following previous works [Kwatny & Piper, 1990; Chang, 2002], this work investigates bifurcations of the power system with three machines and four buses intensively. More specifically, saddle-node bifurcation is first analyzed and then the existence of Hopf bifurcation is obtained through Hopf bifurcation theorem in frequency domain. By the fourth-order harmonic balance method [Moiola & Chen, 1993a, 1993b; Moiola & Chen, 1996; Jing *et al.*, 2002], the periodic oscillations from Hopf bifurcations are also carefully examined and their approximation formulas are given in order to predict the frequencies and amplitudes of these oscillations. Numerical simulations show that the approximations are highly consistent with the numerical solutions of the model system when the bifurcation parameter takes values close to the bifurcation points. Although the approach of frequency domain is an efficient way to approximate oscillations from Hopf bifurcation and predict their frequencies and amplitudes, it is valid only near the bifurcation point. Therefore, numerical simulations are needed to study bifurcations that these periodic oscillations may experience as bifurcation parameter varies. Using numerical methods and the software Auto2007 [Doedel & Oldeman, 2007], we found serval bifurcations of these periodic solutions, including period-doubling bifurcation, torus bifurcation and cyclic fold, and complex dynamical behaviors, including quasi-periodic oscillation and chaotic behavior. These bifurcation points were continued in the parameter space $\Delta P_1$–$\Delta P_2$. These continuations separate the parameter space into six regions, three of which are feasible operating regions. The bifurcation diagram also shows that increases in $\Delta P_2$ may inhibit the occurrence of Hopf bifurcation, torus bifurcation and period-doubling bifurcation. These results provide a better understanding of the dynamics of the power system and also insights into the collapse of power systems.

In the following we first introduce the power system, followed by a conclusion on equilibrium points and their stabilities. Saddle-node bifurcation and Hopf bifurcation are then discussed in Secs. 2.2 and 2.3 separately. The approximation formulas of periodic solutions generated from Hopf bifurcations are given in Sec. 2.4. Our numerical simulations are summarized in Sec. 3 and a conclusion section completes the article.

## 2. The Model and Bifurcation Analysis

### 2.1. *The power system model*

The power system consisting of three machines and four buses with combined constant admittance and P-Q load is illustrated in Fig. 1. Denote the angle and the net power of the $i$th machine by $\delta_i$ $(i = 1, 2, 3)$ and $P_i$ $(i = 1, 2, 3)$, respectively. Taking the first bus as a swing bus [Kwatny & Yu, 1989], the

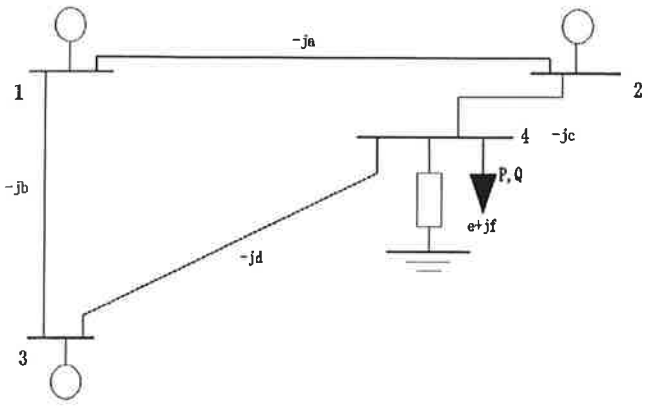


Fig. 1. A four bus power system model.

system can be described by the following differential equations:

$$\begin{cases} \ddot{\bar{\theta}}_1 + \gamma\dot{\bar{\theta}}_1 + 2B_{12}\sin(\bar{\theta}_1) \\ \quad + B_{23}\sin(\bar{\theta}_1 - \bar{\theta}_2) + B_{13}\sin(\bar{\theta}_2) \\ \quad + C_{23}\cos(\bar{\theta}_2 - \bar{\theta}_1) - C_{13}\cos(\bar{\theta}_2) = \Delta P_1 \\ \ddot{\bar{\theta}}_2 + \gamma\dot{\bar{\theta}}_2 + 2B_{13}\sin(\bar{\theta}_2) + B_{23}\sin(\bar{\theta}_2 - \bar{\theta}_1) \\ \quad + B_{12}\sin(\bar{\theta}_1) + C_{23}\cos(\bar{\theta}_2 - \bar{\theta}_1) \\ \quad - C_{12}\cos(\bar{\theta}_1) = \Delta P_2, \end{cases} \tag{1}$$

where $\bar{\theta}_1 = \delta_2 - \delta_1$, $\bar{\theta}_2 = \delta_3 - \delta_1$, $\Delta P_1 = P_2 - P_1$, $\Delta P_2 = P_3 - P_1$. $B_{ij}$ and $C_{ij}$ are transfer conductances. $\gamma$ is the damping factor. Set $x_1 = \bar{\theta}_1$, $x_2 = \dot{\bar{\theta}}_1$, $x_3 = \bar{\theta}_2$, $x_4 = \dot{\bar{\theta}}_2$, and rewrite the system (1) as

$$\begin{cases} \dot{x}_1 = x_2 \\ \dot{x}_2 = \Delta P_1 - (\gamma x_2 + 2B_{12}\sin x_1 \\ \quad + B_{23}\sin(x_1 - x_3) + B_{13}\sin x_3 \\ \quad + C_{23}\cos(x_3 - x_1) - C_{13}\cos x_3) \\ \dot{x}_3 = x_4 \\ \dot{x}_4 = \Delta P_2 - (\gamma x_4 + 2B_{13}\sin x_3 \\ \quad + B_{23}\sin(x_3 - x_1) + B_{12}\sin x_1 \\ \quad + C_{23}\cos(x_3 - x_1) - C_{12}\cos x_1). \end{cases} \tag{2}$$

In the following, the net power $\Delta P_1$ is considered as the bifurcation parameter while other parameters are fixed: $\Delta P_2 = 1.3$, $B_{12} = 0.61$, $B_{13} = B_{23} = 0.4$, $C_{12} = C_{13} = 0.1$, $C_{23} = 1.5$, $\gamma = 0.01$.

By setting the right-hand side of the system (2) equal to zero, we can solve for equilibrium points of the system. Their stabilities are determined by the eigenvalues of the Jacobian matrices at equilibria. Here, we simply summarize our calculations as follows.

**Conclusion 1.** Depending on the parameter $\Delta P_1$, the model system (2) may have

- no equilibrium point in the case of $\Delta P_1 \in (0, 0.106459) \cup (2.36712, +\infty)$;
- two hyperbolic equilibrium points, either a sink and a saddle or two saddles, in the case of $\Delta P_1 \in (0.106459, 1.10117) \cup (1.201861, 1.49080) \cup (1.49080, 2.10269) \cup (2.10269, 2.36712)$;
- four hyperbolic equilibrium points, a sink and three saddles, in the case of $\Delta P_1 \in (1.10117, 1.201861)$;
- a nonhyperbolic equilibrium point $O_i = (x_1^i, x_2^i, x_3^i, x_4^i)$ with eigenvalues having nonzero real parts except one single zero eigenvalue in the case of $\Delta P_1 = \Delta P_1^i$, $i = 1, 2, 3, 6$, where $\Delta P_1^1 = 0.106459$, $\Delta P_1^2 = 1.10117$, $\Delta P_1^3 = 1.201861$, $\Delta P_1^6 = 2.36712$;
- a nonhyperbolic equilibrium point $O_i = (x_1^i, x_2^i, x_3^i, x_4^i)$ with eigenvalues having nonzero real parts except a pair of purely imaginary eigenvalues in the case of $\Delta P_1 = \Delta P_1^i$, $i = 4, 5$, where $\Delta P_1^4 = 1.49080$, $\Delta P_1^5 = 2.10269$.

Here,

$$O_1 = (-0.24298, 0, 0.98944, 0),$$

$$O_2 = (2.92733, 0, -2.68627, 0),$$

$$O_3 = (1.93431, 0, -3.04032, 0),$$

$$O_4 = (0.06608, 0, -0.08168, 0),$$

$$O_5 = (0.65002, 0, 0.02903, 0),$$

$$O_6 = (1.38368, 0, 0.35942, 0).$$

## 2.2. *Saddle-node bifurcation for equilibrium points*

In this subsection, we analyze the existence of saddle-node bifurcation using center manifold theorem and bifurcation theory in time domain. Saddle-node bifurcation may occur if all eigenvalues associated with an equilibrium have nonzero real parts except one simple zero eigenvalue. Conclusion 1 indicates that saddle-node bifurcation may occur in four cases. In the following we discuss these cases separately.

***Case I.*** $\Delta P_1^1 = 0.106459$. In this case, the system (2) admits the equilibrium $O_1 = (x_1^1, x_2^1, x_3^1, x_4^1)$.

To calculate the center manifold of the system (2) at the equilibrium $O_1$, we transform $O_1$ to the origin by setting $y_1 = x_1 - x_1^1$, $y_2 = x_2 - x_2^1$, $y_3 = x_3 - x_3^1$, $y_4 = x_4 - x_4^1$, and $\mu = \Delta P_1 - \Delta P_1^1$. Using the linear transformation matrix $T$,

$$T = \begin{pmatrix} -1.772 \times 10^{-3} & 0.48713 & -0.41453 & -0.41456 \\ 0.66952 & 0 & 4.145 \times 10^{-3} & 0 \\ -1.20 \times 10^{-3} & 0.32991 & -0.90998 & -0.91002 \\ 0.45344 & 0 & 9.10 \times 10^{-3} & 0 \end{pmatrix}$$

and setting

$$\begin{pmatrix} y_1 \\ y_2 \\ y_3 \\ y_4 \end{pmatrix} = T \begin{pmatrix} z_1 \\ z_2 \\ z_3 \\ z_4 \end{pmatrix},$$

we can rewrite the system (2) into the following parameterized system:

$$\begin{pmatrix} \dot{z}_1 \\ \dot{z}_2 \\ \dot{z}_3 \\ \dot{z}_4 \end{pmatrix} = \begin{pmatrix} -0.005 & -1.37442 & 0 & 0 \\ 1.37442 & -0.005 & 0 & 0 \\ 0 & 0 & -0.01 & 0 \\ 0 & 0 & 0 & 0 \end{pmatrix} \begin{pmatrix} z_1 \\ z_2 \\ z_3 \\ z_4 \end{pmatrix} + \begin{pmatrix} f_1(z_1, z_2, z_3, z_4, \mu) \\ f_2(z_1, z_2, z_3, z_4, \mu) \\ f_3(z_1, z_2, z_3, z_4, \mu) \\ f_4(z_1, z_2, z_3, z_4, \mu) \end{pmatrix}, \tag{3}$$

where

$$\begin{aligned} f_1(z_1, z_2, z_3, z_4, \mu) &= 2.16000\mu - 0.05714z_2^2 + 0.04913z_2z_3 - 0.13012z_3^2 + z_1(4.16 \times 10^{-4}z_2 \\ &\quad - 1.79 \times 10^{-4}z_3 - 1.79 \times 10^{-4}z_4) + 0.04913z_2z_4 - 0.26024z_3z_4 - 0.13013z_4^2 + \cdots, \\ f_2(z_1, z_2, z_3, z_4, \mu) &= 7.858 \times 10^{-3}\mu - 2.08 \times 10^{-4}z_2^2 + 1.79 \times 10^{-4}z_2z_3 - 4.73 \times 10^{-4}z_3^2 + 1.79 \times 10^{-4}z_2z_4 \\ &\quad - 9.47 \times 10^{-4}z_3z_4 - 4.73 \times 10^{-4}z_4^2 + \cdots, \\ f_3(z_1, z_2, z_3, z_4, \mu) &= -107.62778\mu + 6.4 \times 10^{-5}z_1^2 + 4.85516z_2^2 - 11.60175z_2z_3 + 46.40414z_3^2 \\ &\quad + z_1(-0.03533z_2 + 0.04221z_3 + 0.04221z_4) \\ &\quad - 11.60233z_2z_4 + 92.81292z_3z_4 + 46.40878z_4^2 + \cdots, \\ f_4(z_1, z_2, z_3, z_4, \mu) &= 107.62240\mu - 6.4 \times 10^{-5}z_1^2 - 4.85492z_2^2 + 11.60117z_2z_3 - 46.40182z_3^2 + z_1(0.03532z_2 \\ &\quad - 0.04220z_3 - 0.04221z_4) + 11.60175z_2z_4 - 92.80828z_3z_4 - 46.40646z_4^2 + \cdots. \end{aligned}$$

When the parameter $\mu = 0$, system (3) admits the zero equilibrium, corresponding to the equilibrium $O_1$ of system (2). To handle this parameterized system (3), we consider the parameter $\mu$ as a new dependent variable, i.e.

$$\dot{\mu} = 0. \tag{4}$$

From the existence theorem for center manifolds, the equilibrium point $(z_1, z_2, z_3, z_4, \mu) = (0, 0, 0, 0, 0)$ of systems (3) and (4) possesses a two-dimensional local center manifold:

$$\begin{aligned} W_{\text{loc}}^{\text{c}}(0) = \{&(z_1, z_2, z_3, z_4, \mu) \in R^5 \mid z_1 = h_1(z_4, \mu), z_2 = h_2(z_4, \mu), z_3 = h_3(z_4, \mu), |z_4| < \delta, \\ &|\mu| < \bar{\delta}, h_i(0, 0) = 0, Dh_i(0, 0) = 0, i = 1, 2, 3\} \end{aligned}$$

for $\delta$ and $\bar{\delta}$ sufficiently small. The dynamics of the systems (3) and (4) near $(z_1, z_2, z_3, z_4, \mu) = (0, 0, 0, 0, 0)$ can be determined by studying the vector field reduced to the center manifold. We now calculate the center manifold. The center manifold must satisfy the following equation:

$$\begin{aligned}&\mathcal{N}(h(z_4, \mu))\\ &\quad = D_{z_4} h(z_4, \mu) \cdot [\hat{A} z_4 + f_4(z_1, z_2, z_3, z_4, \mu)]\\ &\qquad - \hat{B} h(z_4, \mu) - f(z_1, z_2, z_3, z_4, \mu)\\ &\quad = 0,\end{aligned} \tag{5}$$

where

$$h(z_4, \mu) = \begin{pmatrix} h_1(z_4, \mu) \\ h_2(z_4, \mu) \\ h_3(z_4, \mu) \end{pmatrix}, \quad \hat{A} = 0,$$

$$\hat{B} = \begin{pmatrix} -0.005 & -1.37442 & 0 \\ 1.37442 & -0.005 & 0 \\ 0 & 0 & -0.01 \end{pmatrix} \quad \text{and}$$

$$f(z_1, z_2, z_3, z_4, \mu) = \begin{pmatrix} f_1(z_1, z_2, z_3, z_4, \mu) \\ f_2(z_1, z_2, z_3, z_4, \mu) \\ f_3(z_1, z_2, z_3, z_4, \mu) \end{pmatrix}.$$

Assume the center manifold takes the form of

$$\begin{aligned} h(z_4, \mu) &= \begin{pmatrix} h_1(z_4, \mu) \\ h_2(z_4, \mu) \\ h_3(z_4, \mu) \end{pmatrix} \\ &= \begin{pmatrix} a_1 z_4^2 + a_2 z_4 \mu + a_3 \mu^2 + \cdots \\ b_1 z_4^2 + b_2 z_4 \mu + b_3 \mu^2 + \cdots \\ c_1 z_4^2 + c_2 z_4 \mu + c_3 \mu^2 + \cdots \end{pmatrix}. \end{aligned} \tag{6}$$

Substituting (6) into (5), and then equating terms of like powers to zero yield

$$\begin{aligned} h_1(z_4, \mu) &= -1.48273 \times 10^1 z_4 \mu + 8.44735 \mu^2 + \cdots, \\ h_2(z_4, \mu) &= -9.468 \times 10^{-2} z_4^2 + 5.394 \times 10^{-2} z_4 \mu \\ &\quad + 1.161 \times 10^3 \mu^2 + \cdots, \\ h_3(z_4, \mu) &= 4.6408 \times 10^3 z_4^2 - 9.98889 \times 10^7 z_4 \mu \\ &\quad + 1.07501 \times 10^{12} \mu^2 + \cdots. \end{aligned} \tag{7}$$

Therefore, the vector field restricted to the center manifold is given by

$$\begin{cases} \dot{z}_4 = 1.07622 \times 10^2 \mu - 4.64065 \times 10^1 z_4^2 \\ \qquad + 9.27052 \times 10^9 z_4^2 \mu - 4.30705 \times 10^5 z_4^3 \\ \qquad - 9.97698 \times 10^{13} \mu^2 z_4 - 9.99360 \times 10^8 z_4^4 \\ \qquad + 4.30206 \times 10^{13} z_4^3 \mu - 9.25977 \times 10^{17} \mu^2 z_4^2 \\ \qquad + 9.96540 \times 10^{21} \mu^3 z_4 - 5.36241 \times 10^{25} \mu^4 \\ \qquad + \cdots \\ \quad \triangleq F(z_4, \mu) \\ \dot{\mu} = 0. \end{cases} \tag{8}$$

From the center manifold theory, the dynamics in a neighborhood of $(z_1, z_2, z_3, z_4) = (0, 0, 0, 0)$ near $\mu = 0$ for (3) can be determined by the one-parameter ordinary differential equation $\dot{z}_4 = F(z_4, \mu)$ near $\mu = 0$. Recall that the sufficient conditions for an equation $\dot{\xi} = G(\xi, \mu)$, $\xi \in R^1$, $\mu \in R^1$ to undergo a saddle-node bifurcation are $G(0, 0) = 0$, $\frac{\partial G}{\partial \xi}(0, 0) = 0$, $\frac{\partial G}{\partial \mu}(0, 0) \neq 0$, $\frac{\partial^2 G}{\partial \xi^2}(0, 0) \neq 0$. These conditions are satisfied by the $z_4$ equation. In fact,

$$F(0, 0) = 0, \quad \frac{\partial F}{\partial z_4}(0, 0) = 0,$$

$$\frac{\partial F}{\partial \mu}(0, 0) = 1.07622 \times 10^2,$$

$$\frac{\partial^2 F}{\partial {z_4}^2}(0, 0) = -9.28129 \times 10^1.$$

Therefore, $(z_4, \mu) = (0, 0)$ is a saddle-node, that is, the system (2) undergoes a saddle-node bifurcation at $\Delta P_1 = \Delta P_1^1$.

Similarly we investigated the remaining cases: $\Delta P_1^2 = 1.10117$; $\Delta P_1^3 = 1.201861$ and $\Delta P_1^6 = 2.36712$, and summarized our results as follows:

**Conclusion 2.** As the bifurcation parameter $\Delta P_1$ increases, the power system (2) undergoes saddle-node bifurcation at four points, $(O_i, \Delta P_1^i)$, $i = 1, 2, 3, 6$.

### 2.3. *Hopf bifurcation in frequency domain*

In this subsection, we analyze the existence of Hopf bifurcation in frequency domain. Rewrite the system (2) into the following form:

$$\dot{x} = Ax + Bg(y, \nu) \tag{9}$$

together with an output equation

$$y = e = -Cx, \tag{10}$$

where

$$x = \begin{pmatrix} x_1 \\ x_2 \\ x_3 \\ x_4 \end{pmatrix}, \quad \nu = \Delta P_1, \quad e = \begin{pmatrix} e_1 \\ e_2 \\ e_3 \\ e_4 \end{pmatrix}, \quad A = \begin{pmatrix} 1 & 1 & 0 & 0 \\ 0 & -\gamma & 0 & 0 \\ 0 & 0 & 1 & 1 \\ 0 & 0 & 0 & -\gamma \end{pmatrix}, \quad B = C = \begin{pmatrix} 1 & 0 & 0 & 0 \\ 0 & 1 & 0 & 0 \\ 0 & 0 & 1 & 0 \\ 0 & 0 & 0 & 1 \end{pmatrix} \quad \text{and}$$

$$g(y,\nu) = \begin{pmatrix} e_1 \\ \nu + 2B_{12}\sin e_1 + B_{23}\sin(e_1 - e_3) + B_{13}\sin e_3 - C_{23}\cos(e_1 - e_3) + C_{13}\cos e_3 \\ e_3 \\ \Delta P_2 + 2B_{13}\sin e_3 - B_{23}\sin(e_1 - e_3) + B_{12}\sin e_1 - C_{23}\cos(e_1 - e_3) + C_{12}\cos e_1 \end{pmatrix}.$$

Take Laplace transforms on both sides of Eq. (9), and separate its linear part with a transfer function

$$G(s) = C(sI - A)^{-1}B \tag{11}$$

and a memoryless nonlinear part

$$u \triangleq g(e,\nu) \triangleq g(y,\nu) \tag{12}$$

where $s$ is the Laplace variable. Notice that systems (9) and (10) are equivalent to the feedback system with (11) and (12), and the equilibrium point $\hat{e}$ for feedback system with (11) and (12), i.e. the solution $\hat{e}$ of $G(0)g(e,\nu) + e = 0$, is equivalent to the equilibrium point $\hat{x}$ in Eq. (9). Let

$$F(\lambda, s, \nu) = \det(\lambda I - G(s)D_1), \tag{13}$$

where $D_1 = \frac{\partial g}{\partial e}|_{\hat{e}}$, $D_1$ is the Jacobian matrix of the equilibrium point $\hat{e}$.

Mees and Chua [1979], Moiola and Chen [1996] have shown that Hopf bifurcation can occur at the equilibrium point $\hat{e}$ for $\nu = \nu_0$ if $F(\lambda, i\omega, \nu) = 0$ has a single root $\hat{\lambda}(i\omega_0) = -1 + 0i$ for $(\nu_0, \omega_0)$, and $\frac{\partial F(\lambda,i\omega,\nu)}{\partial \omega}|_{(-1,i\omega_0,\nu_0)}$ and $\frac{\partial F(\lambda,i\omega,\nu)}{\partial \nu}|_{(-1,i\omega_0,\nu_0)}$ are nonzero and not parallel, where $i\omega_0$ is the pure imaginary eigenvalue of equilibrium point $\hat{x}$ for model (9) at $\nu = \nu_0$.

Using the above criterion we can determine Hopf bifurcation of system (2). Calculations show that two of the equilibria in Conclusion 1 satisfy the condition of the single root. They are $\hat{e}_1 = (-0.06608, 0, 0.08167, 0)$ at $\nu_{01} = \Delta P_1^4 = 1.49080$, and $\hat{e}_2 = (-0.65002, 0, -0.02903, 0)$ at $\nu_{02} = \Delta P_1^5 = 2.10269$. Further calculations show that:

(1) For $\hat{e}_1$,

$$\left.\frac{\partial F(\lambda, i\omega, \nu)}{\partial \omega}\right|_{(-1,i\omega_{01},\nu_{01})} = -0.01637 - 2.99885 \times 10^{-3} i,$$

$$\left.\frac{\partial F(\lambda, i\omega, \nu)}{\partial \nu}\right|_{(-1,i\omega_{01},\nu_{01})} \approx 9.83890 \times 10^{-3} \quad 0.05518i,$$

$$\omega_{01} = 1.18447;$$

(2) For $\hat{e}_2$,

$$\left.\frac{\partial F(\lambda, i\omega, \nu)}{\partial \omega}\right|_{(-1,i\omega_{02},\nu_{02})} = -0.01798 - 1.97009 \times 10^{-3} i,$$

$$\left.\frac{\partial F(\lambda, i\omega, \nu)}{\partial \nu}\right|_{(-1,i\omega_{02},\nu_{02})} \approx -0.02349 + 0.15348i,$$

$$\omega_{02} = 1.10034.$$

Thus, we have the following conclusion:

**Conclusion 3.** As the bifurcation parameter varies, the nonlinear system consisting of (9), (10) and (12) undergoes Hopf bifurcation at $\nu = \nu_{01}$ (HB$^1$) and at $\nu = \nu_{02}$ (HB$^2$). So does the power system (2).

### 2.4. *The approximation of periodic orbits in frequency domain*

Near a Hopf bifurcation point, the frequency and amplitude of periodic oscillations can be approximated by the harmonic balance approach. In order to reach a high accuracy, we here apply the fourth-order harmonic balance formula to approximate the oscillations generated from Hopf bifurcation at an equilibrium point $\hat{e}$. The approximation formula is given by

$$e(t) \approx \hat{e} + \mathrm{Re}\left(\sum_{k=0}^{4} E^k \exp(ik\hat{\omega}t)\right), \tag{14}$$

where $E^0 = V_{02}\hat{\theta}^2 + V_{04}\hat{\theta}^4$, $E^1 = V_{11}\hat{\theta} + V_{13}\hat{\theta}^3 + V_{15}\hat{\theta}^5$, $E^2 = V_{22}\hat{\theta}^2 + V_{24}\hat{\theta}^4$, $E^3 = V_{33}\hat{\theta}^3 + V_{35}\hat{\theta}^5$, $E^4 = V_{44}\hat{\theta}^4$. $\hat{\omega}$ and $\hat{\theta}$ denote the frequency and amplitude of the periodic solution $e(t)$, respectively. They can be obtained by the following equation:

$$\hat{\lambda}(i\omega) = -1 - \theta^2 Z_1(\omega) - \theta^4 Z_2(\omega). \tag{15}$$

The explicit expressions of $V_{ij}$, $Z_1(\omega)$ and $Z_2(\omega)$ can be found in [Moiola & Chen, 1996; Jing *et al.*, 2002].

Separating the real and imaginary parts of Eq. (15) and eliminating $\theta^4$, we have

$$\begin{aligned}&\mathrm{Re}[\hat{\lambda}(i\omega)+1]\,\mathrm{Im}[Z_2(\omega)] - \mathrm{Re}[Z_2(\omega)]\,\mathrm{Im}[\hat{\lambda}(i\omega)]\\ &\quad = (\mathrm{Re}[Z_2(\omega)]\,\mathrm{Im}[Z_1(\omega)]\\ &\qquad - \mathrm{Re}[Z_1(\omega)]\,\mathrm{Im}[Z_2(\omega)])\theta^2.\end{aligned} \tag{16}$$

There are two cases to be discussed.

***Case (I).*** $\mathrm{Re}[Z_2(\omega)]\,\mathrm{Im}[Z_1(\omega)] - \mathrm{Re}[Z_1(\omega)]\,\mathrm{Im}[Z_2(\omega)] = 0$. In this case, we have

$$\begin{aligned}&\mathrm{Re}[\hat{\lambda}(i\omega)+1]\,\mathrm{Im}[Z_2(\omega)]\\ &\qquad - \mathrm{Re}[Z_2(\omega)]\,\mathrm{Im}[\hat{\lambda}(i\omega)] = 0.\end{aligned} \tag{17}$$

Set $\nu$ to be a number in a small neighborhood of the Hopf bifurcation point $\nu_0$ in Eq. (17) and then numerically solve the equation for $\hat{\omega}$ values that are close to $\omega_0$. Substituting $\hat{\omega}$ value for $\omega$ in Eq. (15), we can obtain a value for $\hat{\theta}^2$. If $\hat{\theta}^2$ is negative, we choose a value for $\nu$ to the other side of $\nu_0$ and repeat the above procedure.

***Case (II).*** $\mathrm{Re}[Z_2(\omega)]\,\mathrm{Im}[Z_1(\omega)] - \mathrm{Re}[Z_1(\omega)]\,\mathrm{Im}[Z_2(\omega)] \neq 0$. In this case, it follows

$$\theta^2 = \frac{\mathrm{Re}[\hat{\lambda}(i\omega)+1]\,\mathrm{Im}[Z_2(\omega)] - \mathrm{Re}[Z_2(\omega)]\,\mathrm{Im}[\hat{\lambda}(i\omega)]}{\mathrm{Re}[Z_2(\omega)]\,\mathrm{Im}[Z_1(\omega)] - \mathrm{Re}[Z_1(\omega)]\,\mathrm{Im}[Z_2(\omega)]}. \tag{18}$$

Similarly, we substitute the formula (18) and a value for $\nu$ into Eq. (15) and calculate $\hat{\omega}$ and $\hat{\theta}^2$.

Following the above procedure, we obtain the following results:

(1) At HB[1], periodic solutions exist for $\nu > \nu_{01} = 1.49080$. When $\nu = 1.49081$, the fourth-order harmonic balance approximation to the periodic solution with $(\hat{\omega}, \hat{\theta}) = (1.18436, 0.07696)$ is given by

$$e(t) \approx \hat{e} + \mathrm{Re}\left(\sum_{k=0}^{4} E^k \exp(ik\hat{\omega}t)\right), \tag{19}$$

where

$$\hat{e} = \begin{pmatrix} -0.06609 \\ 0 \\ 0.08167 \\ 0 \end{pmatrix}, \quad E^0 = 10^{-3} \times \begin{pmatrix} -0.56621 \\ 0 \\ -0.53247 \\ 0 \end{pmatrix},$$

$$E^1 = 10^{-2} \times \begin{pmatrix} -0.00050 - 4.95100i \\ 5.86374 - 0.00059i \\ -0.27167 - 0.25304i \\ 0.29969 - 0.32176i \end{pmatrix}, \quad E^2 = 10^{-3} \times \begin{pmatrix} -0.22176 - 0.02578i \\ 0.06105 - 0.52528i \\ -0.17781 - 0.02265i \\ 0.05366 - 0.42119i \end{pmatrix},$$

$$E^3 = 10^{-5} \times \begin{pmatrix} -0.00136 - 0.04355i \\ 0.15474 - 0.00485i \\ -0.00562 + 0.00578i \\ -0.02055 - 0.01996i \end{pmatrix}, \quad E^4 = 10^{-7} \times \begin{pmatrix} -0.06878 - 0.01048i \\ 0.04964 - 0.32585i \\ -0.04018 - 0.00689i \\ 0.03262 - 0.19036i \end{pmatrix}.$$

(2) At $HB^2$, periodic solutions exist for $\nu < \nu_{02} = 2.10269$. When $\nu = 2.10266$, the fourth-order harmonic balance approximation to the periodic solution with $(\hat{\omega}, \hat{\theta}) = (1.10033, 0.03151)$ is given by

$$e(t) \approx \hat{e} + \mathrm{Re}\left(\sum_{k=0}^{4} E^k \exp(ik\hat{\omega}t)\right), \tag{20}$$

where

$$\hat{e} = \begin{pmatrix} -0.64998 \\ 0 \\ -0.02902 \\ 0 \end{pmatrix}, \quad E^0 = 10^{-4} \times \begin{pmatrix} -0.50953 \\ 0 \\ -0.27786 \\ 0 \end{pmatrix},$$

$$E^1 = 10^{-2} \times \begin{pmatrix} -0.00033 - 1.63204i \\ 1.79578 - 0.00036i \\ -0.01917 - 1.35177i \\ 1.48740 - 0.02110i \end{pmatrix}, \quad E^2 = 10^{-4} \times \begin{pmatrix} -0.11948 - 0.00184i \\ 0.00405 - 0.26294i \\ -0.05090 - 0.00076i \\ 0.00166 - 0.11200i \end{pmatrix},$$

$$E^3 = 10^{-7} \times \begin{pmatrix} -0.00402 - 0.14140i \\ 0.46676 - 0.01327i \\ -0.00477 - 0.14875i \\ 0.49101 - 0.01575i \end{pmatrix}, \quad E^4 = 10^{-9} \times \begin{pmatrix} -0.03910 - 0.00026i \\ 0.00115 - 0.17211i \\ -0.02305 - 0.00001i \\ 0.00006 - 0.10145i \end{pmatrix}.$$

## 3. Numerical Simulations

The approximate formulas (19) and (20) are valid only in some neighborhoods of the Hopf bifurcation points $HB^1$ and $HB^2$. Therefore, in this section, we first illustrate that the bifurcated periodic solutions can be well-approximated near the bifurcation points and then utilize numerical simulations of the system (2) and the software Auto2007 to further study bifurcations that the periodic solutions may undergo. We use the abbreviations: X ($x_1$), Y ($x_2$), Z ($x_3$), MAX(X) (maximum of $x_1$), SNB (saddle-node bifurcation), HB (Hopf bifurcation), CFB (cyclic fold bifurcation), PDB (period-doubling bifurcation), TR (torus bifurcation).

The numerical solutions of the system (2) near two Hopf bifurcations are illustrated in Figs. 2(a) and 2(b) (green circles), respectively. The corresponding approximations by the formulas (19)

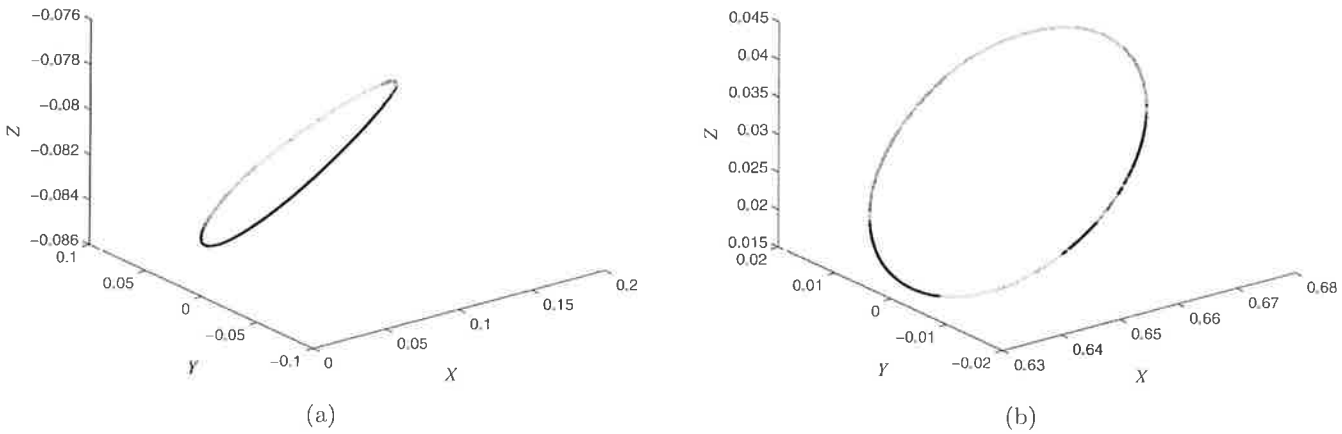


Fig. 2. The projections of periodic solutions near two Hopf bifurcation points $HB^1$ and $HB^2$. (a) $\Delta P_1 = 1.49081$ and (b) $\Delta P_1 = 2.10266$.

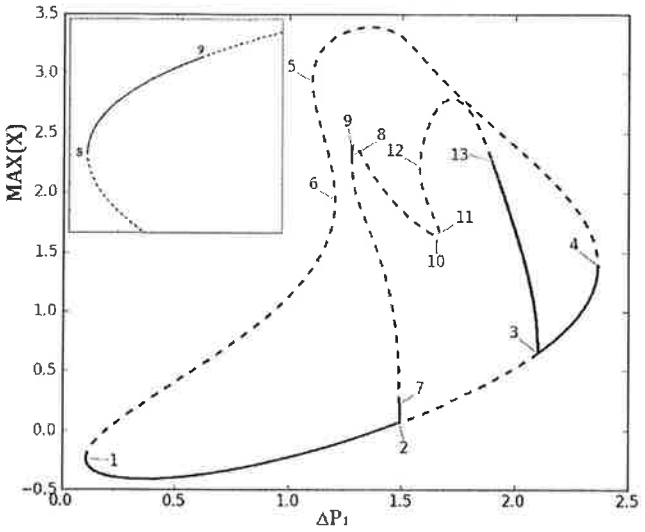


Fig. 3. Bifurcation diagram of $\Delta P_1$ versus MAX(X).

and (20) are also shown in the figures (black circles). One can see that the approximations are quite close to the numerical solutions, indicating the validness of the formulas. The frequencies predicted by the frequency domain approach are also highly consistent with those obtained through Auto2007. Predicted frequencies of the solutions are 1.18436 for $\Delta P_1 = 1.49081$ and 1.10033 for $\Delta P_1 = 2.10266$ while the frequencies given by Auto2007 are 1.18435 and 1.10033, respectively.

To further study the bifurcations of periodic solutions, we use Auto2007 to draw the bifurcation diagram in the $\Delta P_1$-MAX(X) plane. Figure 3 demonstrates the diagram and the bifurcation points are summarized in Table 1. The solid and the dashed curves in Fig. 3 represent the stable and the unstable equilibrium points or periodic solutions, respectively.

From Fig. 3 one can see that the power system first undergoes six bifurcations labeled as $SNB^1$, $HB^2$, $HB^3$, $SNB^4$, $SNB^5$ and $SNB^6$. For $0.106459 < \Delta P_1 < 1.49080$, there is a stable equilibrium point (lower left in Fig. 3). As $\Delta P_1$ increases, the equilibrium point loses its stability through a supercritical Hopf bifurcation at $HB^2$ and a family of stable periodic solutions emerges. With a further increase in $\Delta P_1$, the equilibrium point regains its stability at $\Delta P_1 = 2.10269$ through a supercritical Hopf bifurcation $HB^3$, and remains stable until $SNB^4$ at $\Delta P_1 = 2.36712$.

The branches of periodic solutions emerging from Hopf bifurcations are also illustrated in Fig. 3. The branch of periodic solutions bifurcated from $HB^2$ finally coincides with that from $HB^3$. Between $HB^2$ and $HB^3$, i.e. in the "Hopf window", periodic solutions undergo seven types of bifurcations: $CFB^7$, $CFB^8$, $TR^9$, $PDB^{10}$, $CFB^{11}$, $CFB^{12}$, $PDB^{13}$.

On the branch emerging from $HB^2$, the stable periodic solution bifurcated from $HB^2$ loses its stability through a cyclic fold bifurcation $CFB^7$ and remains unstable till another cyclic fold bifurcation $CFB^8$ is met at $\Delta P_1 = 1.27511$. As the bifurcation parameter $\Delta P_1$ increases, a pair of complex conjugate Floquet multipliers associated to the periodic solution, $0.85045 \pm 0.52607i$, crosses the unit circle from the inside, so that a torus bifurcation $TR^9$ occurs at $\Delta P_1 = 1.27545$, and a quasi-periodic solution arises from $TR^9$. Figure 4 shows the projection of the quasi-periodic solution at $\Delta P_1 = 1.276$. Our calculations show that there are bistable ranges for $\Delta P_1 \in (1.27511, 1.27545)$ where a stable equilibrium and a stable periodic solution coexist, and $\Delta P_1 \in (1.27545, 1.49080)$ where a stable equilibrium point coexists with a quasi-periodic solution. Further numerical simulations show that chaotic oscillations exist for $\Delta P_1 \in (1.2763, 1.278)$. At $\Delta P_1 = 1.2778$, the chaotic attractor with Lyapunov exponents $\{0.02391, 0, -0.016285, -0.027097\}$ is illustrated in Fig. 5. From $TR^9$ to $PDB^{13}$, the periodic solution remains unstable, and has no qualitative change.

Due to supercritical Hopf bifurcation $HB^3$, the stable periodic solutions generate from $HB^3$. With a decrease in $\Delta P_1$, one of the multipliers crosses the unit circle at $-1$ from the inside to the outside for $\Delta P_1 = 1.89672$, so that a period-doubling bifurcation $PDB^{13}$ occurs, and the stable periodic solution loses its stability. Figures 6(a) and 6(b) show the stable period-one orbit for $\Delta P_1 = 1.9$ and the period-two orbit for $\Delta P_1 = 1.896$.

To further study the impact of the parameters $\Delta P_1$ and $\Delta P_2$ on the dynamics of the power

Table 1. Bifurcation points and $\Delta P_1$ values in Fig. 3.

| | $SNB^1$ | $HB^2$ | $HB^3$ | $SNB^4$ | $SNB^5$ | $SNB^6$ | $CFB^7$ | $CFB^8$ | $TR^9$ | $PDB^{10}$ | $CFB^{11}$ | $CFB^{12}$ | $PDB^{13}$ |
|---|---|---|---|---|---|---|---|---|---|---|---|---|---|
| $\Delta P_1$ | 0.106459 | 1.49080 | 2.10269 | 2.36712 | 1.10117 | 1.20186 | 1.49085 | 1.27511 | 1.27545 | 1.65211 | 1.66579 | 1.57931 | 1.89672 |

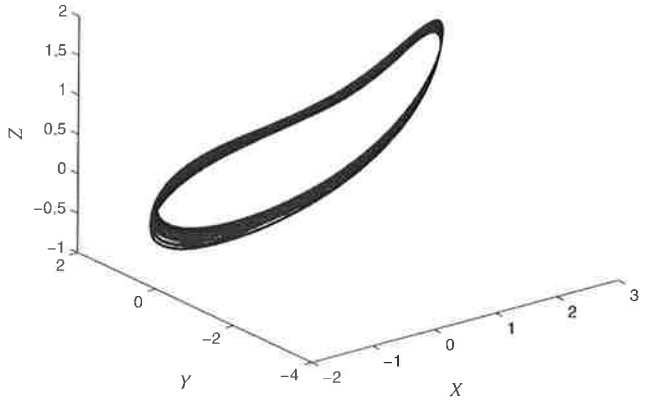


Fig. 4. The projection of a quasi-periodic trajectory for $\Delta P_1 = 1.276$.

system (2), we utilize the software Auto2007 again to continue the above bifurcation points and obtain bifurcation loci in the $\Delta P_1$–$\Delta P_2$ plane. These bifurcation loci are illustrated in Fig. 7. The saddle-node bifurcation points $SNB^1$, $SNB^4$, $SNB^5$ and $SNB^6$ are on the curves $L1$ and $L2$, and the Hopf bifurcation points $HB^2$ and $HB^3$ are on the curve $L3$. The curves $L4$ and $L5$ are the loci of torus bifurcation and period-doubling bifurcation, respectively.

The bifurcation loci in Fig. 7 simply separate the parameter space into six regions, where the dynamical behavior of the power system (2) is numerically examined. Region I, surrounded by $L2$ and the $\Delta P_1$-axis, is an operation region of the power system and the system has a stable equilibrium point. Region II, enclosed by $L3$, $L4$ and the $\Delta P_1$-axis, is the second operation region. The dynamical behavior of the power system in this region is complicated. A stable equilibrium point and quasi-periodic solution exist simultaneously. Chaotic behavior can be observed in this region too.

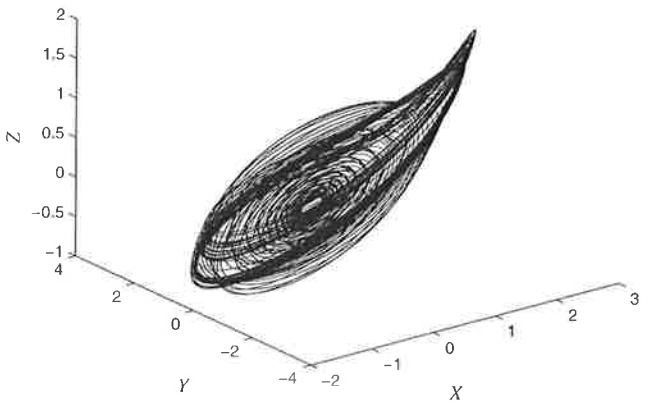


Fig. 5. The projection of a chaotic trajectory for $\Delta P_1 = 1.2778$.

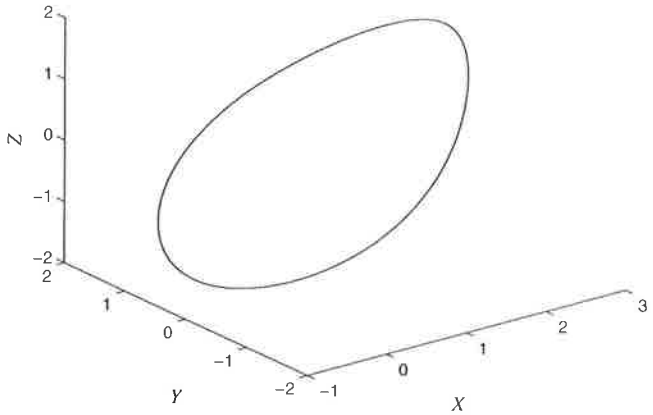


(a)

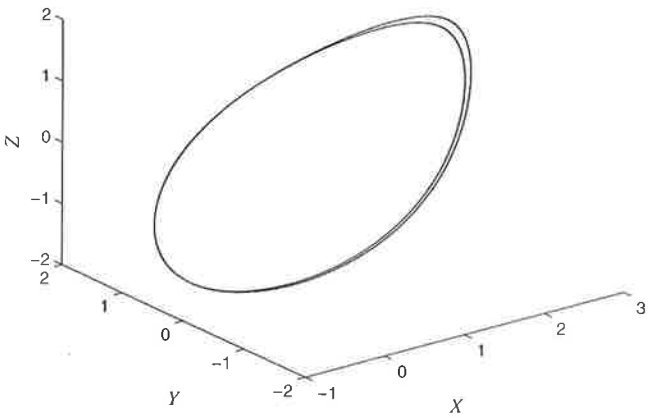


(b)

Fig. 6. Periodic orbits. (a) Period-one orbit for $\Delta P_2 = 1.9$ and (b) period-two orbit for $\Delta P_2 = 1.896$.

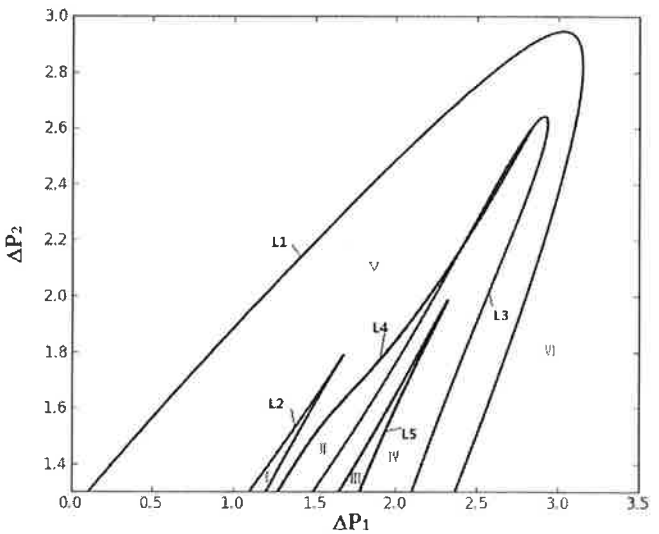


Fig. 7. Continuation of bifurcation points in the parameter space $\Delta P_1$ and $\Delta P_2$.

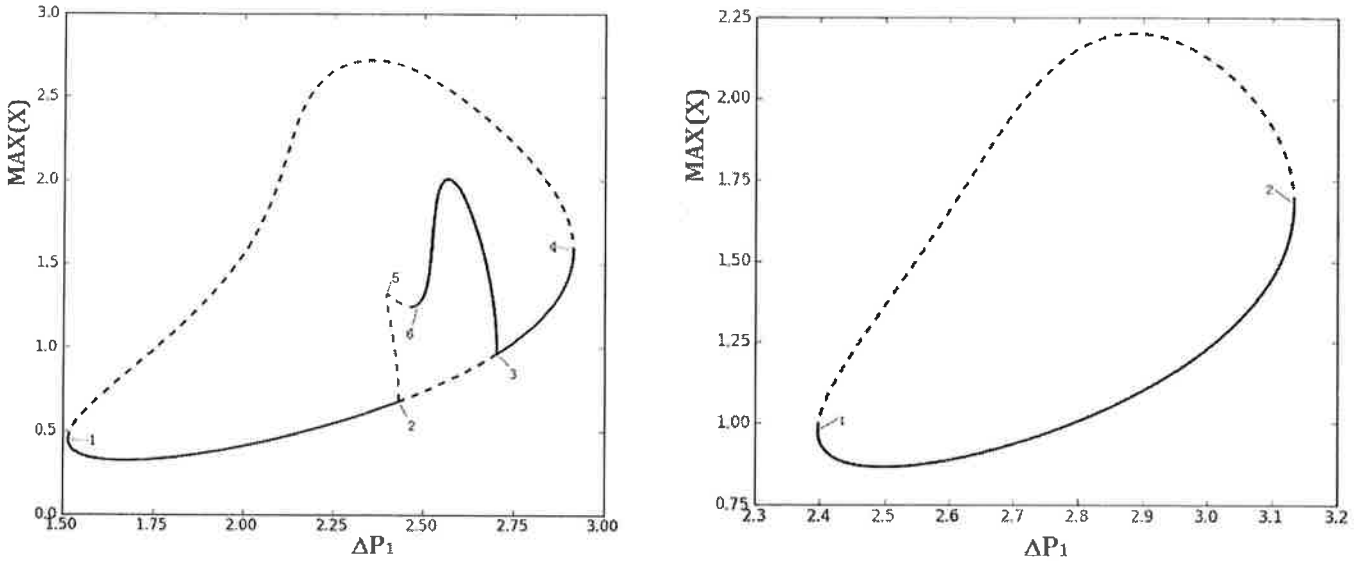


(a) (b)

Fig. 8. Bifurcation diagrams. (a) $\Delta P_2 = 2.2$ with $SNB^1$, $HB^2$, $HB^3$, $SNB^4$, $CFB^5$ and $TR^6$ and (b) $\Delta P_2 = 2.7$ with $SNB^1$ and $SNB^2$, in which there is no dynamic bifurcation.

Region III is enclosed by $L5$ and the horizontal axis. In the region, all equilibrium points are unstable and period-two solutions can be found. The power system exhibits periodic oscillations in the region between $L3$ and $L5$ (Region IV in Fig. 7) and equilibria are unstable. Region V (see Fig. 7) is the third operation region of the system, where a stable equilibrium and stable periodic solution can coexist. There is no equilibrium point in Region VI.

One can see from Fig. 7 that $\Delta P_2$ can inhibit the occurrences of dynamic bifurcations, i.e. Hopf bifurcation, torus bifurcation and period-doubling bifurcation. Let $\Delta P_1$ be a constant. With an increase in $\Delta P_2$, the period-doubling bifurcation first is prevented to occur, then the torus bifurcation and the Hopf bifurcation are also inhibited by increasing $\Delta P_2$. In addition, the unstable region of the equilibrium point between two saddle-node bifurcations becomes smaller when $\Delta P_2$ increases, which are illustrated in Figs. 8(a) and 8(b). Thus the increase in $\Delta P_2$ contributes to the stable region of the equilibrium point and the feasible region of the system.

## 4. Conclusions

For the power system (2), the existence of saddle-node bifurcation and Hopf bifurcation was analytically studied in time domain and in frequency domain, respectively. Fourth-order harmonic balance method allowed us to obtain highly accurate predictions on frequencies, amplitudes and the explicit approximation expressions for periodic solutions emerging from Hopf bifurcation. Our numerical simulations indicate the method is valid in some neighborhoods of the bifurcation points. To further study possible bifurcation of periodic solutions away from bifurcation points, we utilized the software Auto2007 to draw bifurcation diagrams and performed extensive numerical simulations. It was found that the periodic solutions undergo various type of bifurcations, including cyclic fold bifurcation, period-doubling bifurcation and torus bifurcation. We also found complex dynamical behaviors, including quasi-periodic orbits, period-one orbit and period-two orbit, and chaotic behavior. By continuing bifurcation points in parameter space $\Delta P_1$ and $\Delta P_2$ (see Fig. 7), we noticed that an increase in $\Delta P_2$ contributes to the feasible region of the power system. All the results improve our understanding to the dynamics of the power system and provide insight into the instability of power systems.

## References

Abed, E. H., Wang, H. O., Alexander, J. C., Hamdan, A. M. A. & Lee, H.-C. [1993] "Dynamic bifurcation in a power system model exhibiting voltage collapse," *Int. J. Bifurcation and Chaos* **3**, 1169–1176.

Ayasun, S., Nwankpa, C. O. & Kwatny, H. G. [2004] "Computation of singular and singularity induced

bifurcation points of differential-algebraic power system model," *IEEE Trans. Circuits Syst.* **51**, 1525–1538.

Chang, Y. [2002] "Bifurcation and chaos theories of dynamical systems and its applications," Institute of Mathematics, Chinese Academy of Mathematics and Systems Sciences, Ph.D. thesis (in Chinese).

Doedel, E. J. & Oldeman, B. E. [2007] "Auto-07p: Software for continuation and bifurcation problems in ordinary differential equations," available via http://cmvl.cs.concordia.ca/auto.

Harb, A. & Jabbar, N. A. [2003] "Controlling Hopf bifurcation and chaos in a small power system," *Chaos Solit. Fract.* **18**, 1055–1063.

Huang, M., Tse, C. K., Wong, S. C., Wan, C. & Ruan, X. B. [2013] "Low-frequency Hopf bifurcation and its effects on stability margin in three-phase PFC power supplies connected to non-ideal power grid," *IEEE Trans. Circuits Syst.* **60**, 3328–3340.

Jing, Z. J., Wang, J. L. & Chen, L. N. [2002] "Computation of limit cycle via higher order harmonic balance approximation and its application to a 3-bus power system," *IEEE Trans. Circuits Syst.* **49**, 1360–1369.

Kwatny, H. G. & Yu, X. M. [1989] "Energy analysis of load-induced flutter instability in classical models of electric powder networks," *IEEE Trans. Circuits Syst.* **36**, 1544–1557.

Kwatny, H. G. & Piper, G. E. [1990] "Frequency domain analysis of Hopf bifurcations in electric power networks," *IEEE Trans. Circuits Syst.* **37**, 1317–1321.

Kwatny, H. G., Fischl, R. F. & Nwankpa, C. O. [1995] "Local bifurcation in power systems: Theory, computation, and application," *Proc. IEEE* **83**, 1456–1482.

Li, Y. H., Chiang, H. D., Li, H., Chen, Y. T. & Huang, D. H. [2008] "Applying bifurcation analysis to determine optimal placements of measurement devices for power system load modeling," *Int. J. Bifurcation and Chaos* **18**, 2111–2121.

Mees, A. I. & Chua, L. O. [1979] "The Hopf bifurcation theorem and its applications to nonlinear oscillations in circuits and systems," *IEEE Trans. Circuits Syst.* **26**, 235–254.

Mendoza-Armenta, S., Fuerte-Esquivel, C. R. & Becerril, R. [2013] "A numerical study of the effect of degenerate Hopf bifurcations on the voltage stability in power systems," *Electr. Pow. Syst. Res.* **101**, 102–109.

Moiola, J. L. & Chen, G. R. [1993a] "Frequency domain approach to computation and analysis of bifurcations and limit cycles: A tutorial," *Int. J. Bifurcation and Chaos* **3**, 843–867.

Moiola, J. L. & Chen, G. R. [1993b] "Computations of limit cycles via higher order harmonic balance approximation," *IEEE Trans. Automat. Contr.* **38**, 782–790.

Moiola, J. L. & Chen, G. R. [1996] *Hopf Bifurcation Analysis: A Frequency Domain Approach* (World Scientific, Singapore).

Pirooz, A. S., Iravani, R. & Tate, J. E. [2015] "Dynamic stability enhancement of a DC-segmented AC power system via HVDC operating-point adjustment," *IEEE Trans. Pow. Deliv.* **30**, 657–665.

Rakshit, B., Apratim, M. & Banerjee, S. [2010] "Bifurcation phenomena in two-dimensional piecewise smooth discontinuous maps," *Chaos* **20**, 033101.

Sangrody, R. A., Nazarzadeh, J. & Nikravesh, K. Y. [2012] "Bifurcation and Lyapunov's exponents characteristics of electrical scalar drive systems," *Pow. Electron.* **5**, 1236–1244.

Tavora, C. J. & Smith, O. T. [1972] "Equilibrium analysis of power system," *IEEE Trans. Pow. Appl. Syst.* **91**, 1131–1137.

Wang, S. B., Du, P. W. & Zhou, N. [2014] "Power system transient stability analysis through a homotopy analysis method," *Nonlin. Dyn.* **76**, 1079–1086.

Zhang, Y. S. & Chiang, H. D. [2011] "Local bifurcation boundary and steady-state security boundary in large electric power systems: Numerical studies," *Int. J. Bifurcation and Chaos* **21**, 647–662.